SCIENCE CHINA
Chemistry

•ARTICLES•

June 2021 Vol.64 No.6: 1020–1030
https://doi.org/10.1007/s11426-020-9964-x

Dual drug delivery system with flexible and controllable drug ratios for synergistic chemotherapy

Yalan Tu[1†], Rui Zheng[1†], Fangzhou Yu[2], Xuan Xiao[3], Maoling Jiang[3,4] & Youyong Yuan[1,2,5*]

[1]*Institutes for Life Sciences, School of Medicine, South China University of Technology, Guangzhou 510006, China;*
[2]*National Engineering Research Center for Tissue Restoration and Reconstruction, South China University of Technology, Guangzhou 510006, China;*
[3]*Key Laboratory of Biomedical Materials and Engineering of the Ministry of Education, South China University of Technology, Guangzhou 510006, China;*
[4]*Key Laboratory of Biomedical Engineering of Guangdong Province and Innovation Center for Tissue Restoration and Reconstruction, South China University of Technology, Guangzhou 510006, China;*
[5]*Bioland Laboratory (Guangzhou Regenerative Medicine and Health Guangdong Laboratory), Guangzhou 510005, China*

Received December 10, 2020; accepted February 22, 2021; published online April 27, 2021

Determination of whether multidrug nanocarriers can deliver and release loaded drugs at a predefined synergistic ratio to target cancer cells is crucial. Although there are many successful applications for delivery of multiple drugs, most current carriers are unable to achieve coordinated loading and release, leading to a drug release ratio that disagrees with the predefined loading ratio. In this work, a simple dual-drug delivery system with a flexible and controllable drug release ratio was constructed to deliver two anticancer drugs, doxorubicin (DOX) and curcumin (CUR). The drug ratio of DOX and CUR can be easily tuned for an enhanced synergistic effect, and the drugs can be released at predesigned ratios due to synchronous drug activation and nanoparticle collapse. Drug release at predefined ratios for synergistic anticancer therapy was demonstrated *via in vitro* and *in vivo* experiments. Therefore, the dual drug delivery system developed here provides a simple and efficient strategy for combination chemotherapy.

nanomedicine, drug delivery system, combination therapy, synergistic chemotherapy

Citation: Tu Y, Zheng R, Yu F, Xiao X, Jiang M, Yuan Y. Dual drug delivery system with flexible and controllable drug ratios for synergistic chemotherapy. *Sci China Chem*, 2021, 64: 1020–1030, https://doi.org/10.1007/s11426-020-9964-x

1 Introduction

Chemotherapy, a major clinical therapeutic approach for cancer treatment, usually suffers from many application restrictions due to severe side effects and acquired drug resistance (ADR) [1,2]. To improve therapy and overcome multidrug resistance, combination chemotherapy that comprises multiple non-cross-resistant anticancer agents has become a common solution [3–5]. Compared with a single agent, a synergistic effect can be induced through the complementary molecular activity of multiple drugs [6]. However, other issues still need to be addressed with regard to combination chemotherapy. One of the most crucial problems is delivery of the drugs to the target at the correct ratio [7]. Previous studies have revealed that the synergistic effect of combination chemotherapy largely depends on the ratio of multiple drugs at the target location, and multidrug antagonism may appear if the ratio is not appropriate [8]. On the other hand, there is always an optimal ratio within the scope of synergy [9]. Therefore, codelivery of drugs to cancer cells at predefined synergistic ratios is vital for combination

†These authors contributed equally to this work.
*Corresponding author (email: yuanyy@scut.edu.cn)

chemotherapy.

Traditional cocktail administration has the problem of significantly different physicochemical properties between the combined drugs and therefore suffers from different pharmacokinetics in systemic circulation [7]. The application of advanced nanocarriers to deliver multiple drugs has become a popular trend, and many carriers achieve better tumor targeting or reduce toxic side effects, thereby improving therapeutic outcomes to a certain extent [10,11]. However, although many advanced nanoparticles have been successfully applied for delivery of multiple drugs, few can maintain a constant and precise drug release ratio due to the different physicochemical properties of the drugs and premature drug release [9,12,13]. To solve this problem, new strategies involving conjugation of polymers with drugs at precise ratios through a responsive linker to form polyprodrugs have been developed for combination cancer chemotherapy [14–20]. For instance, a polymerization prodrug macromonomer dual-drug delivery platform was developed for combination chemotherapy by Johnson *et al*. [16]. Although this strategy was demonstrated to be an efficient pathway for combination chemotherapy, most platforms still suffer from the limitation that the activated drugs may not be released at predefined synergistic ratios because the polymer nanocarriers still exist after cleavage of the responsive linker, which blocks drug release through noncovalent binding. The noncovalent binding force between drugs and carriers is often different according to differences in drug physicochemical properties, such as hydrophobicity, ultimately leading to different release rates. Therefore, developing a prodrug with synchronous drug activation and polymer degradation may achieve consistent drug loading and release at predefined synergistic ratios.

In this work, a simple and innovative dual-drug delivery system with a flexible and controllable drug release ratio was constructed to deliver two anticancer drugs, doxorubicin (DOX) and curcumin (CUR), for combination chemotherapy (Scheme 1). The two model drugs show a synergistic effect: CUR can enhance the antitumor efficiency of DOX by downregulating the expression of P-glycoprotein (P-gp) in cancer cells [21]. To endow the system with tumor targeting ability, we conjugated the drug with polyethylene glycol (PEG) *via* a reduction-responsive cleavable disulfide bond. In aqueous environments, the PEG-modified amphiphilic prodrugs PEG-ss-DOX and PEG-ss-CUR can co-assemble into nanoparticles. The resulting prodrug nanoparticles, denoted as $SNP_{DOX/CUR}$, can accumulate in tumor tissue through the enhanced permeability and retention (EPR) effect [22]. With the high intracellular glutathione (GSH) concentration in cancer cells, the disulfide linker in the prodrug can be cleaved, resulting in simultaneously drug activation and nanoparticle collapse. In this $SNP_{DOX/CUR}$ delivery system, the DOX to CUR drug loading ratio can be tuned for an enhanced synergistic effect *via* a flexible and controllable method of adjusting the two prodrug feeding ratios during nanoparticle preparation. More importantly, due to synchronous drug activation and nanoparticle collapse, the effects of the different binding forces between the carriers and drugs are eliminated. Therefore, DOX and CUR loading and release at predefined ratios can be achieved using our design, which provides a simple and efficient strategy for combination chemotherapy.

2 Experimental

2.1 Materials

DOX was purchased from Dalian Meilun Biotechnology (Dalian, China). CUR was purchased from Arocss (USA). 2,2′-Dithiodiethanol was purchased from Aladdin. Triton X-100, 11-chloro-1,1′-di-*n*-propyl-3,3,3′,3′-tetramethyl-10,12-trimethyleneindatricarbocyanine iodide (IR-780) and 3-(4,5-dimethylthiazol-2-yl)-2,5-diphenyltetrazolium bromide (MTT) were purchased from Sigma-Aldrich (USA). Carboxylic acid functionalized methoxyl polyethylene glycol (mPEG45-COOH) was purchased from JenKen Co. Ltd. (China). Triphosgene, *N*,*N*′-dicyclohexylcarbodiimide (DCC), 4-dimethylaminopyridine (DMAP), and glutathione (GSH) were purchased from ENERGY (Shanghai, China). Tetrahydrofuran (THF), *N*,*N*-dimethylformamide (DMF), dichloromethane (DCM), triethylamine (TEA), ethyl ether, *p*-nitrobenzoyl chloride (NPC), dimethyl sulfoxide (DMSO), methanol, acetonitrile trifluoroacetic acid (TFA), and acetic acid were purchased from China National Pharmaceutical Group Corporation. Dulbecco's modified Eagle's medium (DMEM), trypsin-EDTA and penicillin-streptomycin were obtained from Gibco BRL (Eggenstein, Germany). Fetal bovine serum (FBS) was obtained from ExCell Biology, Inc. (Shanghai, China). Hoechst 33342 was purchased from Life Technologies (China).

2.2 Synthesis of prodrugs

2.2.1 Synthesis of mPEG-ss-OH

2,2′-Dithiodiethanol (468 mg, 3.04 mmol) and DCC (123.6 mg, 0.60 mmol) were dissolved in 30 mL of dry DCM. Then, 5 mL of dry DCM containing $mPEG_{45}$-COOH (600 mg, 0.30 mmol) was slowly added into the mixture in an ice bath. The reaction was carried out at room temperature for 24 h. Thereafter, the mixture was concentrated and precipitated to excess of cold ethyl ether for three times. Drying in vacuum for 24 h, the product mPEG-ss-OH as white solid was obtained (428 mg, 66.3%). ^{1}H NMR (400 MHz, chloroform-*d*): δ 4.44 (t, J=6.6 Hz, 2H), 3.88 (t, J=6.0 Hz, 2H), 3.65 (s, 180H), 3.38 (s, 3H), 2.96 (t, J=6.6 Hz, 2H), 2.88 (t, J=6.0 Hz, 2H).

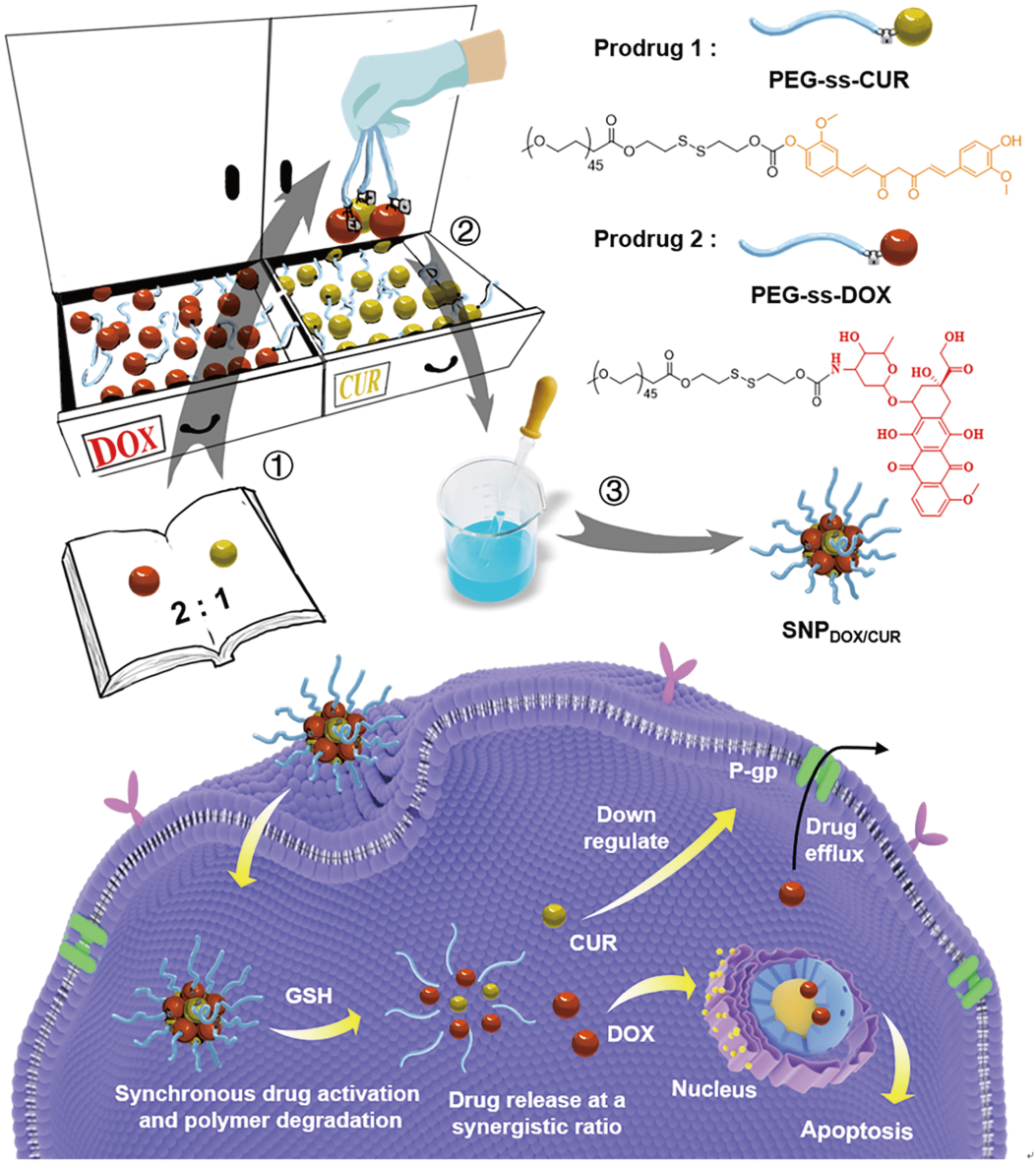

Scheme 1 Schematic illustration of the dual prodrug with a predefined drug ratio for synergistic chemotherapy to reverse drug resistance. Step 1: determination of the optimal drug combination ratio according to the literature or pre-experiment results; Step 2: modification of the prodrug feeding ratio according to the predefined optimal drug combination ratio; Step 3: sensitive prodrug self-assembly and nanoparticle formation in an aqueous environment (color online).

2.2.2 *Synthesis of PEG-ss-CUR*

mPEG-ss-OH (150 mg, 0.07 mmol) and triphosgene (20 mg, 0.068 mmol) were dissolved in dry DCM (8 mL), then the mixture of TEA (70 mg, 0.69 mmol) and DMAP (15 mg, 0.12 mmol) in DCM (2 mL) was added slowly. The mixture was stirred for 1 h under a nitrogen atmosphere. Subsequently, CUR (77.3 mg, 0.21 mmol) dissolved in 5 mL of DCM was added and the mixture was stirred for 48 h. Thereafter, the mixture was concentrated and precipitated to excess of cold ethyl ether for three times. Then, the precipitation was dissolved in 5 mL of THF, and the product was purified by gel chromatography (Bio-Beads S-X1 Support). Drying in vacuum for 24 h, the product PEG-ss-CUR as yellow solid was obtained (131 mg, 73%). ^{1}H NMR (400 MHz, chloroform-*d*): δ 7.72–7.54 (m, 1H), 7.22–6.88 (m, 3H), 6.68–6.38 (m, 1H), 5.86 (d, *J*=13.8 Hz, 1H), 4.47 (dt, *J*=31.0, 6.9 Hz, 4H), 4.09–3.79 (m, 4H), 3.64 (s, 180H), 3.38 (d, *J*=1.1 Hz, 3H), 2.99 (ddd, *J*=29.3, 14.4, 6.8 Hz, 3H).

2.2.3 *Synthesis of PEG-ss-DOX*

mPEG-ss-OH (150 mg, 0.07 mmol), TEA (70 mg, 0.69 mmol) are dissolved in dry DCM (8 mL), then 2 mL of DCM containing NPC (135 mg, 0.73 mmol) was added slowly and the mixture was stirred for 24 h at room temperature. Thereafter, the mixture was concentrated and precipitated to excess of cold ethyl ether for three times. The

obtained precipitation was dried in vacuum overnight. All of precipitation was then dissolve in 5 mL of dry DMF and 2 mL of dry DMF containing DOX (40 mg, 0.074 mmol) and TEA (20 mg, 0.198 mmol) was added into the solution slowly. The mixture was stirred for 24 h at room temperature. The reaction solution was then concentrated to 2 mL and the product was purified by gel chromatography (Bio-Beads S-X1 Support). Drying in vacuum for 24 h, the product PEG-ss-DOX as red solid was obtained (129 mg, 68%). ^{1}H NMR (400 MHz, chloroform-*d*): δ 13.99 (s, 1H), 13.28 (s, 1H), 8.06 (d, *J*=7.7 Hz, 1H), 7.80 (t, *J*=8.1 Hz, 1H), 7.41 (d, *J*=8.5 Hz, 1H), 5.51 (s, 1H), 5.42 (d, *J*=8.6 Hz, 0H), 5.32 (s, 1H), 4.77 (s, 1H), 4.62 (s, 0H), 4.41 (s, 2H), 4.25 (s, 1H), 4.13 (d, *J*=35.0 Hz, 3H), 3.64 (d, *J*=1.5 Hz, 183H), 3.06 (d, *J*=19.3 Hz, 1H), 2.98–2.83 (m, 3H), 2.36 (d, *J*=14.7 Hz, 1H), 2.17 (d, *J*=13.4 Hz, 1H), 1.45–1.06 (m, 3H).

2.3 Cell culture and tumor model

Human breast cancer doxorubicin-resistant cell line MCF-7/ADR cells were cultured in DMEM medium with 10% FBS, 1% penicillin-streptomycin. Cells were cultured in 5% CO_2 and 21% O_2 incubator at 37 °C. Female BALB/c nude mice (20±2 g, 5–6 weeks old) were purchased from Beijing Vital River Laboratory Animal Technology Co., Ltd. (Beijing, China). MCF-7/ADR cells (5×10^6) were injected into the right mammary fat pads with subcutaneous injection of β-estradiol to establish an orthotopic MCF-7/ADR tumor model. After the tumor volumes reached to 100 or 500 mm^3, the mice were used for subsequent experiments. At the end of experiments, all mice were killed by CO_2 inhalation. All animal experiments were approved by the Ethics Committee of the South China University of Technology.

2.4 High-performance liquid chromatography analysis

High-performance liquid chromatography (HPLC) analysis was performed on an Agilent Technologies 1200 Series system. The isocratic mobile phase consisted of acetonitrile and acetic acid aqueous solution (5%, *v*/*v*) in volume ratio of 75:25. TFA (0.1%, *v*/*v*) was added to the mobile phase to prevent peak tailing. The fluorescence detector was set at 420 nm of excited light wavelength and 540 nm of emission light wavelength to detect CUR, 495 nm of excited light wavelength and 595 nm of emission light wavelength to detect DOX.

2.5 Preparation of the sensitive prodrug nanoparticles $SNP_{DOX/CUR}$

The sensitive prodrug nanoparticles SNPDOX/CUR with drug loading ratio of DOX to CUR at 2:1 (corresponding DOX percent 67%) were prepared using the classic nanoprecipitation method. Under stirring (1,000 r min^{-1}), the mixture solution of PEG-ss-CUR (30.0 mg, loading CUR 4.0 mg or 0.011 mmol) and PEG-ss-DOX (60.0 mg, loading DOX 11.9 mg or 0.022 mmol) in DMSO (5 mL) was dropwise to 25 mL of deionized water. Subsequently, the formed NPs dispersion was transferred to dialysis tube (molecular weight cut off, MWCO 3,500), dialyzing against deionized water for 24 h to remove DMSO, the NPs were finally obtained. $SNP_{DOX/CUR}$ with different drug loading ratios was also prepared by adjusting the corresponding feed ratio of PEG-ss-CUR and PEG-ss-DOX during the nanoprecipitation process.

2.6 Preparation of the control encapsulated dual-drug loading nanoparticles $ENP_{DOX/CUR}$

The control encapsulated loading dual-drug nanoparticles ($ENP_{DOX/CUR}$) were also prepared using the nanoprecipitation method. Under stirring (1,000 r min^{-1}), the mixture of poly (ethylene glycol) methyl ether-*block*-poly(lactide) (PEG_{5k}-*b*-PLA_{8k}, 40.0 mg), CUR (1.0 mg), DOX (4.2 mg) in 2 mL DMSO was added slowly to 10 mL of deionized water. Subsequently, the formed NPs dispersion was transferred to dialysis tube (MWCO 3,500), dialyzing against deionized water for 24 h to remove DMSO, the $ENP_{DOX/CUR}$ was finally obtained. HPLC analysis was used to confirm that the drug loading molar ratio of DOX to CUR is the predefined 2:1.

2.7 Investigation of reduction-responsive behavior of the prodrug PEG-ss-DOX and PEG-ss-CUR

The 5 mg of PEG-ss-DOX or PEG-ss-CUR was dissolved in 1 mL of DMF containing 10 mM DTT, placing at room temperature for 2 and 8 h. The molecular weight distribution of the polymer after incubated with DTT was examined by GPC analysis.

2.8 *In vitro* drugs release

The $SNP_{DOX/CUR}$ and $ENP_{DOX/CUR}$ with the same drug loading molar ratio 2:1 of DOX to CUR were prepared according to the method described above and the total drug concentration (DOX plus CUR) was adjusted to 0.5 mg mL^{-1} (DOX 373 μg mL^{-1} plus CUR 127 μg mL^{-1}). To quantitatively determine the release of DOX and CUR, 1 mL of the NPs solution was taken in the dialysis membrane tubing (MWCO 3,500 Da) and the tubing was immersed in 25 mL of phosphate buffer saline (PBS) containing different concentration of GSH (0, 1 and 10 mM) and 0.05% Triton X-100, in a shaking water bath at 37 °C. At predetermined time points, the external buffer of 100 μL was collected and freeze-dried. Finally, the drug was extracted with acetonitrile and detected by HPLC analysis.

The cumulative DOX&CUR release was calculated as

follows:

$$\text{Cumulative release (\%)} = \left(M_t / M\right) \times 100$$

where the M_t is the amount of DOX or CUR released from NPs at time t; M is the amount of DOX or CUR in the NPs.

2.9 *In vitro* cytotoxicity

The MCF-7/ADR cells were seeded in a 96-well plate with a density of 5×10^3 cells per well. After the incubation in 100 μL of DMEM medium containing 10% FBS for 24 h, a fixed amount of NPs (or drug) dispersed in 100 μL of fresh medium was added and the cells were allowed to incubate for another 24 or 48 h, replacing the medium with 100 μL of fresh medium containing MTT (0.5 mg mL^{-1}), incubating for another 4 h, and replacing the medium with 100 μL DMSO, shaking for 30 min. Absorption at 570 nm was measured by Synergy HT multi-mode microplate reader. The average value of five independent experiments was collected and the cell viability was calculated as follows:

$$\text{Cell viability (\%)} = (\text{Abs. treated} / \text{Abs. control}) \times 100$$

where the Abs. control is the absorption obtained in the absence of the NPs, and the Abs. treated is absorption obtained in the presence of the NPs.

CI values, defined as the sum of the two ratios of the median effect doses (D_1, D_2) of each drug alone to the median effect doses (D_{m1}, D_{m2}) of each drug in the combination, were plotted against drug effect levels (IC_x values) at various cell viability points.

2.10 Intracellular drugs release

MCF-7/ADR cells were seeded in 24-well plates at a density of 1×10^5 cells per well and incubated overnight. The cells were washed with PBS and treated with NPs in culture medium with equivalent DOX at a concentration of 5 μg mL^{-1}. Cells were incubated at 37 °C for different periods of time, washed twice with cold PBS, and lysed in deionized water at ultrasound for 1 h with three freeze-thaw cycles. The cell lysates were then freeze dried and dissolved in acetonitrile. DOX and CUR concentrations in cell lysates were measured by HPLC analyses and normalized to the total cellular protein content of the cells, which was determined by the BCA Protein Assay Kit (Pierce, Rock-ford, IL).

2.11 *In vitro* cellular uptake

The cellular uptake of $SNP_{DOX/CUR}$ was investigated by using a confocal laser scanning microscope (CLSM). Briefly, MCF-7/ADR cells were seeded into a 35 mm glass-bottom dishes at a density of 1×10^5 cells per well and incubated overnight. The cells were treated with $SNP_{DOX/CUR}$ (1 μg mL^{-1} DOX). After incubating for 0.5, 2, 4, 8 and 12 h, the cells were then washed with PBS and studied by CLSM.

2.12 *In vivo* imaging and bio-distribution study

The biodistribution of $ENP_{DOX/CUR}$ and $SNP_{DOX/CUR}$ loaded with IR-780 *in vivo* were examined using MCF-7/ADR tumor bearing Balb/c nude mouse model. To establish the orthotopic tumor model, each nude mouse was injected with 5×10^6 of MCF-7/ADR cells on the right mammary gland with β-estradiol treated. After tumor volume reached 200 mm^3, the tumor-bearing mice were randomly grouped, and intravenously injected with 200 μL of $SNP_{CUR/DOX}$ at IR780 dose of 1.5 mg kg^{-1}. The body fluorescence images were collected at 24 h after injection using *in vivo* Xtreme (Bruker, German). The mice were sacrificed at 24 h after administration for *ex vivo* examining the IR780 distribution in major organs.

2.13 Antitumor efficacy and safety evaluation

Balb/c nude mice (20–25 g) bearing MCF-7/ADR tumor under breast were used as animal model to investigate the antitumor efficacy *in vivo*. When tumors grew to about 100 mm^3 in size, 7 days after inoculation of the cancer cells, the mice were randomly divided into 3 groups and were given three injections of drugs intravenously on day 0, 3 and 6, with the day of the first injection counted as day 0. The tumor size and body weight were then monitored every two days for two weeks. The recipes for the 3 groups were as follows: (a) saline, (b) $ENP_{DOX/CUR}$ (5.00 mg DOX/kg, 6.03 mg CUR/kg), (c) $SNP_{DOX/CUR}$ (5.00 mg DOX/kg, 6.03 mg CUR/kg). Both of $ENP_{DOX/CUR}$ and $SNP_{DOX/CUR}$ have a same drug loading ratio according to predesign (molar ratio of DOX:CUR=2:1). All the mice were administrated three consecutive injections and the tumor growth was monitored by measuring perpendicular diameters using a caliper and tumor volume was calculated as follows:

$$V=W^2\times L/2$$

where W and L are the shortest and longest diameters, respectively.

At day 12, mice were sacrificed, and tumor was excised to intuitionally evaluate the tumor inhibition. In order to investigate the safety of formulations, main organs (heart, liver, spleen, lung, kidney) and tumor were collected, fixed in 4% paraformaldehyde solution, and then embedded in paraffin, sliced and stained with hematoxylin and eosin (H&E) to evaluate potential toxicity for main organs and apoptosis degree for cancer cells.

2.14 Drug release ratio in tumor tissue

Balb/c nude mice (20–25 g) bearing MCF-7/ADR tumor

under breast were used as animal model to investigate drug release ratio in tumor tissue. When tumors grew to about 500 mm^3 in size, mice were randomly divided in two groups (n=3) and were given injections of drugs intravenously. The recipes for the two groups were $ENP_{DOX/CUR}$ (5.00 mg DOX/kg, 6.03 mg CUR/kg) and $SNP_{DOX/CUR}$ (5.00 mg DOX/kg, 6.03 mg CUR/kg). Both of two groups have a same drug loading ratio according to fore design (molar ratio of DOX: CUR=2:1). Two days later after injections, the mice were sacrificed and the tumor tissue (about 0.5 g) were excised and homogenized in PBS solution. The supernatant was obtained after homogenate and centrifugation at 15,000 r min^{-1} for 2 h. After the supernatant was freeze-dried for 48 h, 1 mL of acetonitrile was used to extract the free DOX and CUR. The content of free DOX and CUR were detected by HPLC.

2.15 Statistical analysis

All the data were presented as mean ± standard deviation. One-way analysis of variance (ANOVA) was used to assess the significance of the difference. Statistical significance was set at *p<0.05, **p<0.01 and ***p<0.005.

3 Results and discussion

3.1 Optimal combination ratio of free DOX to CUR

We first studied the cytotoxicity profiles of free DOX and CUR at different ratios toward michigan cancer foundation-7/acquired drug resistance (MCF-7/ADR) cells using an MTT study. As depicted in Figure 1(a), 67% DOX, corresponding to a 2:1 ratio of DOX to CUR, showed considerably higher cytotoxicity than most of the other drug ratios after both 24 and 48 h of incubation. To identify the best drug ratio, we carried out combination index (CI) determinations. The CI values were derived from dose-effect profiles of a given drug combination and were plotted against the drug effect level. Such a plot can provide quantitative information about the extent of drug interactions; a lower CI value indicates a more significant synergistic effect. The difference in the synergistic effects was clearly revealed by the CI value after 24 and 48 h of incubation (Figure 1(b)). Among all the drug ratios, the synergistic effect of DOX at 67% was the best at all drug effect levels from 30% to 70% after both 24 and 48 h of incubation. These results confirmed that for synergistic activity, the best DOX to CUR combination ratio is 2:1.

3.2 Synthesis and characterization of prodrug

We synthesized the prodrugs PEG-ss-CUR and PEG-ss-DOX through the method shown in Scheme S1 (Supporting Information online), and the dual-drug delivery system was built as shown in Scheme 1. Hydrophobic DOX and CUR were chosen as synergetic chemotherapeutic drugs and conjugated with hydrophilic PEG through a response-cleavable disulfide bond. The final products were characterized *via* ^{1}H NMR (Figures S1–S3, Supporting Information online) and gel permeation chromatography (GPC) studies (Figure

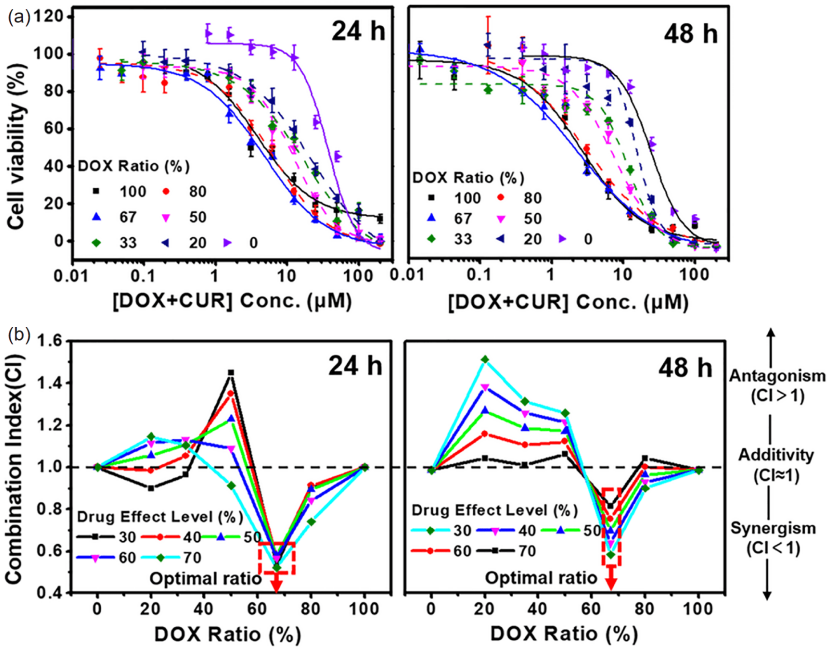

Figure 1 (a) *In vitro* cytotoxicity of DOX and CUR at various ratios after incubation for 24 or 48 h. (b) The CI values of DOX and CUR at various ratios after incubation for 24 or 48 h (color online).

S4). Two characteristic absorption peaks (420 and 495 nm) appeared in the ultraviolet-visible spectroscopy (UV-Vis) absorption spectrum of PEG-ss-CUR and PEG-ss-DOX solution, confirming prodrug exactly contain CUR and DOX (Figure S5). The reduction-sensitive dual drug nanoparticles, termed $SNP_{DOX/CUR}$, were self-assembled by employing intermolecular interactions between the hydrophobic chemotherapeutic drugs. The morphology and hydrodynamic diameter of $SNP_{DOX/CUR}$ was studied by transmission electron microscope (TEM) and dynamic light scattering (DLS) (Figure 2(c)), and there was no significant size change in the absence of GSH, indicating the morphology of $SNP_{DOX/CUR}$ was typical and stable (Figure S6). According to the design, the disulfide group in the prodrugs PEG-ss-CUR and PEG-ss-DOX can be cleaved under reductive conditions, such as exposure to GSH or DTT, and then, the free drug is activated and released (Scheme S2). We first employed GPC and DLS to confirm the reduction-responsive cleavability of the prodrugs PEG-ss-CUR and PEG-ss-DOX. As shown in Figure 2 (a) and Figure S7, after PEG-ss-CUR or PEG-ss-DOX was incubated with DTT (10 mM) in DMF for 8 h, their molecular weight decreased dramatically to ~2,000 g mol^{-1}, which is close to the molecular weight of PEG. We further studied the drugs release and activation by HPLC analysis. As shown in Figure 2(b), the retention time and peak type of DOX and CUR released from prodrug PEG-ss-DOX and PEG-ss-CUR is exactly the same as free standard DOX and CUR, indicating that the drugs released from prodrug were the pure drugs without any chemical residues. It is necessary to explain that because free standard CUR contains three derivatives (mixture of curcumin, demethoxycurcumin and bisdemethoxycurcumin), the HPLC profile is multi peak. Moreover, $SNP_{DOX/CUR}$ rapidly swelled and dissociated, showing a change in hydrodynamic diameter from 119 to 1,080 nm after incubation with GSH for 8 h due to hydrophobic drug release and assembly (Figure 2(c)).

3.3 Studies of drug release in solution

This reduction-responsive degradation of $SNP_{DOX/CUR}$ was further investigated by examining DOX and CUR release profiles in PBS (pH 7.4) containing different concentrations of GSH (0, 1 and 10 mM). As shown in Figure 2(d), $SNP_{DOX/CUR}$ demonstrated almost negligible drug release in the absence of GSH. At a relatively low concentration of GSH (1 mM), sustained DOX and CUR release behavior of $SNP_{DOX/CUR}$ was observed, while at a relatively high concentration of GSH (10 mM), the release action became distinctly faster, owing to significant degradation of $SNP_{DOX/CUR}$. It is crucial that $SNP_{DOX/CUR}$ can release two drugs at precise and stable drug ratios as a result of synchronous drug activation and nanocarrier collapse. We prepared control CUR and DOX co-encapsulated nanoparticles, denoted as $ENP_{DOX/CUR}$, using poly(ethylene glycol)-*block*-poly(lactic) (PEG-*b*-PLA) as carrier. HPLC characterization results (Figure S8) show $ENP_{DOX/CUR}$ had a specific drug loading ratio (DOX: CUR=2:1, or DOX loading ratio=67%), which was the same ratio as $SNP_{DOX/CUR}$. Figure 2(e) shows the cumulative re-

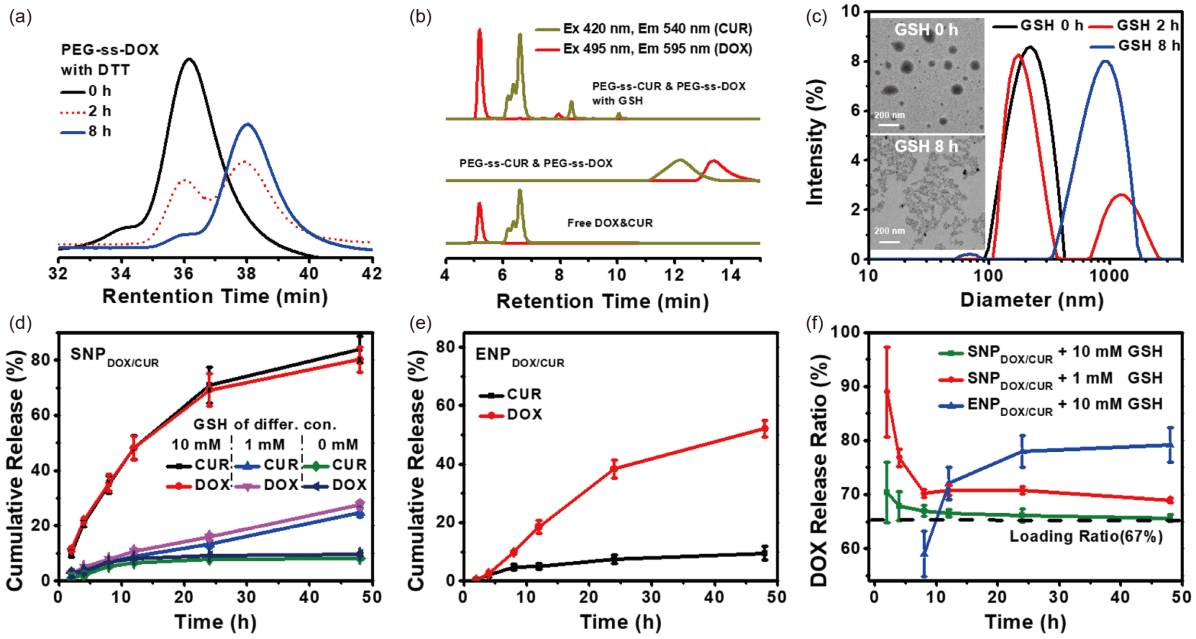

Figure 2 (a) GPC profiles of PEG-ss-DOX before and after incubation with DTT (10 mM); (b) HPLC profiles of PEG-ss-CUR and PEG-ss-DOX before or after incubation with GSH (10 mM) for 12 h; (c) size and morphology of $SNP_{DOX/CUR}$ before or after incubation with GSH (10 mM); (d) CUR and DOX release profiles from $SNP_{DOX/CUR}$ incubated with different concentrations of GSH (0, 1, and 10 mM); (e) CUR and DOX release profiles from $ENP_{DOX/CUR}$ incubated with GSH (10 mM); (f) drug release ratio profiles of $SNP_{DOX/CUR}$ and $ENP_{DOX/CUR}$ (color online).

lease rates of DOX and CUR from $ENP_{DOX/CUR}$ were obviously different, and the release rate of CUR was significantly lower than that of DOX. We estimated that this should be due to that the two drugs are both encapsulated in $ENP_{DOX/CUR}$ through noncovalent hydrophobic interactions but CUR is more hydrophobic than DOX, leading to tighter binding with carrier's hydrophobic block, making CUR more difficult to release from nanocarriers and thus leads to non-synchronous release rates of DOX and CUR. As a result, the release ratio of DOX to CUR was inconsistent with the loading ratio (DOX:CUR=2:1) for the control $ENP_{DOX/CUR}$ (Figure 2(f)).

3.4 Confirmation of $SNP_{DOX/CUR}$ synergistic effect

To confirm the drug loading ratio 2:1 of DOX to CUR was still the best synergistic drug ratio for $SNP_{DOX/CUR}$, $SNP_{DOX/CUR}$ was prepared with different drug loading ratios by controlling the prodrug PEG-ss-CUR and PEG-ss-DOX feeding during the nanoparticle preparation process. The cytotoxicity profiles of $SNP_{DOX/CUR}$ in MCF-7/ADR cells were studied by MTT assay. As shown in Figure 3(a), 67% DOX loading ratio still showed considerable cytotoxicity compared with most of the other ratios. The CI values were also calculated to evaluate the synergistic effect. As shown in Figure 3(c), CI values of $SNP_{DOX/CUR}$ with DOX at 67% were less than 1 and lowest among all the other drug loading ratios, demonstrating that $SNP_{DOX/CUR}$ with 67% DOX still had the best synergistic effect in MCF-7/ADR cells. In the meantime, we studied the cytotoxicity of control $ENP_{DOX/CUR}$ to MCF-7/ADR cells (Figure 3(b)) and demonstrated more significant synergistic effect of $SNP_{DOX/CUR}$ than $ENP_{DOX/CUR}$ by comparing CI values (Figure 3(d)).

3.5 Intracellular drug release ratio studies

To study whether $SNP_{DOX/CUR}$ can be internalized by MCF-7/ADR cells and whether the drugs can be released from $SNP_{DOX/CUR}$ in response to the reductive intracellular microenvironment, we incubated MCF-7/ADR cells with $SNP_{DOX/CUR}$ for different times (0.5, 2, 4, 8, 12 h). Red fluorescence indicating the presence DOX was detected *via* CLSM. As shown in Figure 4(a), the fluorescence representing DOX gradually intensified as $SNP_{DOX/CUR}$ was internalized by cells with the release of DOX. Moreover, quantitative evaluation of the intracellular content of released DOX and CUR after incubation was also performed. First, we collected and lysed cells at different incubation time intervals from 4 to 24 h, and the intracellular levels of DOX and CUR released from nanoparticles were then quantitatively determined by HPLC analysis of drug content in the cell lysates and finally normalized to the total cellular protein content. As shown in Figures 4(b, c), the intracellular concentration of DOX and CUR increased with incubation time, but only $SNP_{DOX/CUR}$ maintained a relatively accurate and stable drug release ratio consistent with the predesigned drug loading ratio (Figure 4(d)).

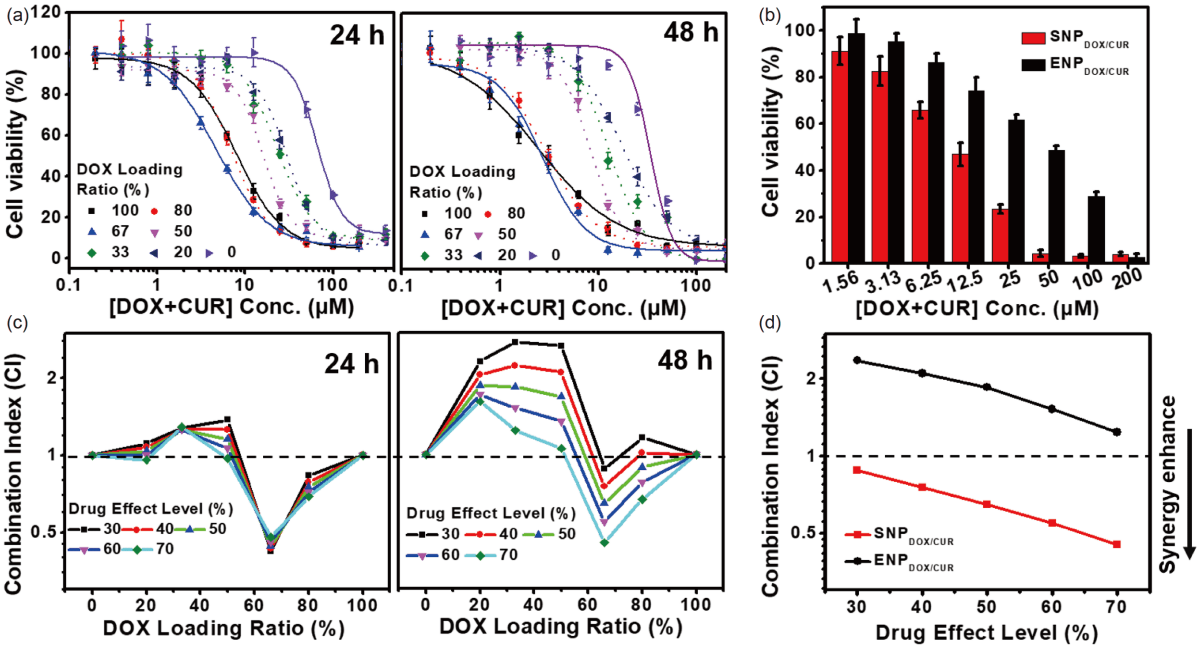

Figure 3 (a) *In vitro* cytotoxicity of $SNP_{DOX/CUR}$ with different drug loading ratios after incubation for 24 or 48 h; (b) *in vitro* cytotoxicity of $SNP_{DOX/CUR}$ and $ENP_{DOX/CUR}$ with DOX loading ratio 67% after incubation for 48 h; (c) the CI values of $SNP_{DOX/CUR}$ with different drug loading ratios after incubation for 24 or 48 h; (d) the CI values of $SNP_{DOX/CUR}$ or $ENP_{DOX/CUR}$ with DOX loading ratio 67% after incubation for 48 h against different drug effect levels (color online).

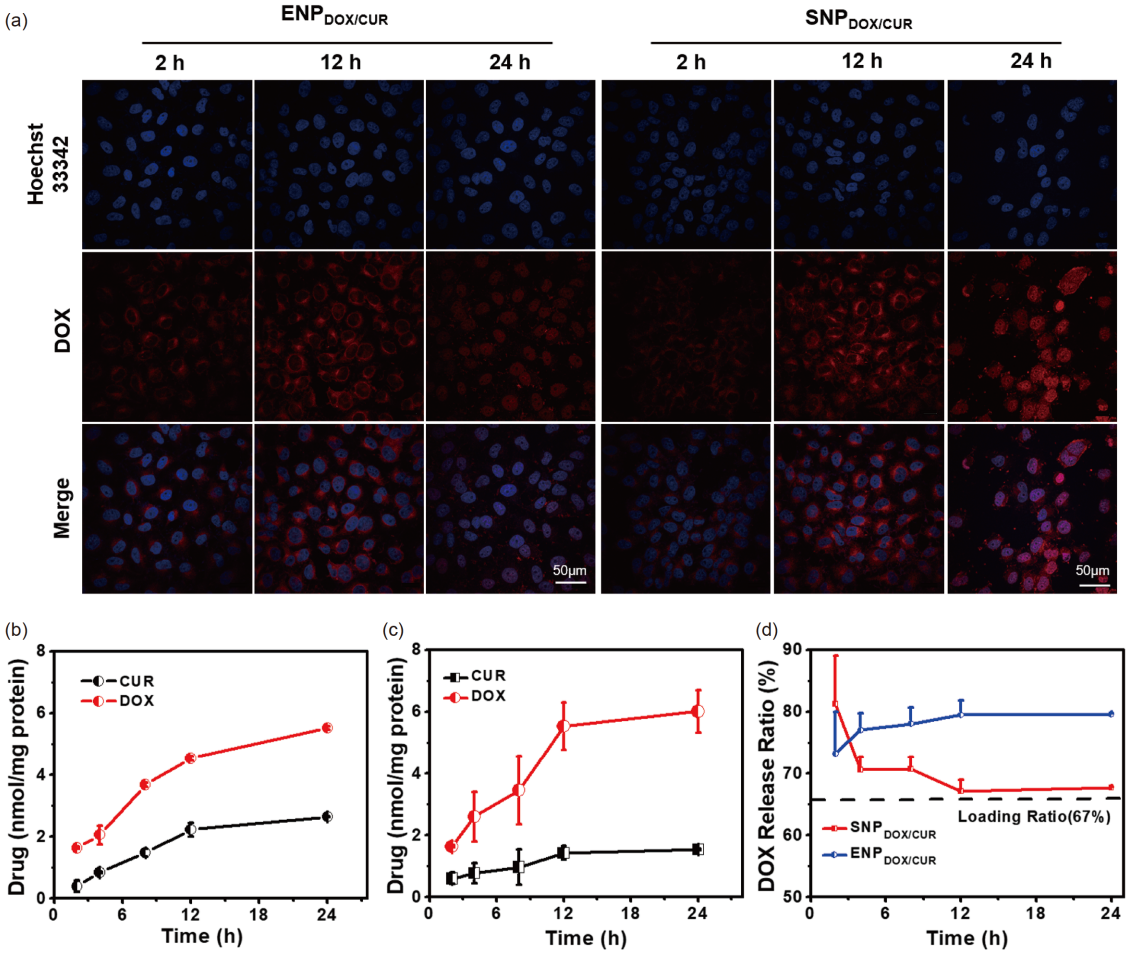

Figure 4 (a) Confocal images of MCF-7/ADR cells incubated with $SNP_{DOX/CUR}$ for different time. Red fluorescence indicates DOX and blue fluorescence indicates Hoechst stained nucleus. (b) Intracellular CUR and DOX release profiles of $SNP_{DOX/CUR}$ at different time points. (c) Intracellular CUR and DOX release profiles of $ENP_{DOX/CUR}$ at different time points. (d) Intracellular drug release ratio profiles of $SNP_{DOX/CUR}$ and $ENP_{DOX/CUR}$ at different time points (color online).

3.6 Biodistribution studies

Nanoparticles can accumulate in tumor tissue through the enhanced permeability and retention (EPR) effect. The *in vivo* biodistribution of $ENP_{DOX/CUR}$ and $SNP_{DOX/CUR}$ was assessed in nude mice bearing MCF-7/ADR tumors as a model. To compare the tumor tissue enrichment ability at the same imaging level, $ENP_{DOX/CUR}$ and $SNP_{DOX/CUR}$ were loaded with the near infrared dye IR-780 using the same encapsulation method. As shown in Figure 5(a), both $ENP_{DOX/CUR}$ and $SNP_{DOX/CUR}$ accumulated and remained at the tumor site for up to 24 h after intravenous injection. To further confirm the tissue distribution, the mice were sacrificed and the tumors and major organs were collected for *ex vivo* imaging 24 h after injection (Figure 5(c)). The quantified IR-780 fluorescence intensities in the different organs and tumors are shown in Figure 5(b). IR-780-loaded $ENP_{DOX/CUR}$ and $SNP_{DOX/CUR}$ showed similar enrichment in tumor tissue. This evidence suggests that both $ENP_{DOX/CUR}$ and $SNP_{DOX/CUR}$ effectively accumulated in the tumor site through the EPR effect, and no obvious difference in their biodistribution was observed. Hence, the results provide us with comparable fundamentals to assess the therapeutic efficiency of the two formulations *in vivo*.

3.7 Treatment and drug release ratio in tumor tissue

We next evaluated the tumor growth suppression efficacy of $SNP_{DOX/CUR}$ using an MCF-7/ADR tumor model of breast cancer developed by injection of MCF-7/ADR cells into the left breast of nude mice. Seven days after inoculation of the MCF-7/ADR cells, the tumors grew to approximately 100 mm^3. Then, the mice were randomly divided into 3 groups (n=5) and the mice were given an intravenous tail vein injection with (a) PBS, (b) $ENP_{DOX/CUR}$ or (c) $SNP_{DOX/CUR}$, and the DOX and CUR doses in the $ENP_{DOX/CUR}$ and $SNP_{DOX/CUR}$ groups were the same, at 5.00 mg DOX/kg and 1.69 mg CUR/kg, corresponding to a molar ratio of 2:1 DOX

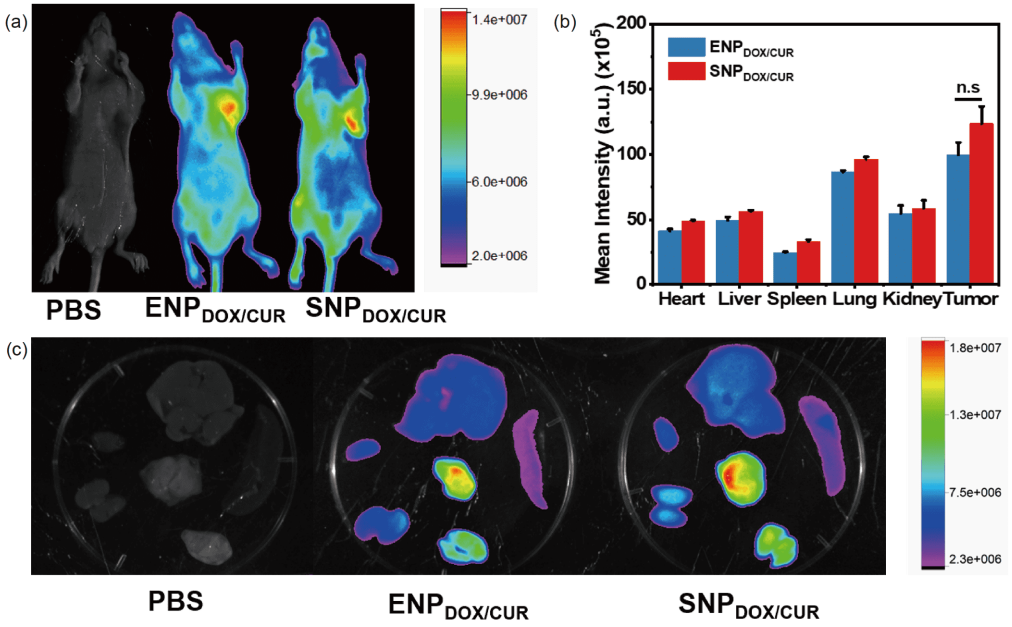

Figure 5 (a) *In vivo* fluorescence images of MCF-7/ADR tumor-bearing nude mice obtained 24 h after intravenous injection of PBS, $ENP_{DOX/CUR}$ and $SNP_{DOX/CUR}$ loaded with the infrared dye IR-780; (b) quantification of fluorescence intensities in tumors and normal organs (n=3); (c) *ex vivo* fluorescence imaging of tumors and normal organs collected from the mice 24 h after intravenous injection (color online).

to CUR. Drugs were injected on days 0, 3 and 6, for a total of three injections, and the day of the first injection was considered day 0. Tumor size and body weight were then monitored every two days for two weeks. As shown in Figure 6(a–d), compared with the control groups that received $ENP_{DOX/CUR}$ or PBS injection, mice in the $SNP_{DOX/CUR}$ group showed more significant tumor growth suppression. Moreover, to verify that the controllable drug release ratio was the most significant cause of the antitumor effect of $SNP_{DOX/CUR}$, we collected and homogenized all tumor tissues. After the extraction process was performed on the homogenate, quantitative HPLC analysis was used to detect the content of free DOX and CUR released from $SNP_{DOX/CUR}$ and $ENP_{DOX/CUR}$. The results shown in Figure 6(e, f) indicated that the $SNP_{DOX/CUR}$ drug release ratio is close to the drug loading ratio (molar DOX:CUR=2:1, or DOX 67%), which is also the predesigned and optimal drug release ratio. On the other hand, *in vivo* fluorescence images showing that the $ENP_{DOX/CUR}$ and $SNP_{DOX/CUR}$ groups had a similar *in vivo* distribution due to the EPR effect (Figure 5) illustrated that there was no significant difference in nanoparticle tumor tissue enrichment. The greater antitumor efficacy of $SNP_{DOX/CUR}$ could be further due to the optimal drug release ratio. Combined with the *in vitro* release profile (Figure 2), we speculated that the drug release ratio of $ENP_{DOX/CUR}$ was significantly lower than the loading and injection ratio because a considerable proportion of the DOX had been released from $ENP_{DOX/CUR}$ during long systemic circulation before nanoparticle enrichment in tumor tissues due to the relatively weak hydrophobicity of DOX compared with CUR, which resulted in a lower DOX to CUR release ratio than the loading ratio when injected. These results confirm that drugs can be released at predefined ratios from $SNP_{DOX/CUR}$ to achieve controllable and stable synergistic anticancer therapy. Additionally, histological analysis *via* H&E staining of the major organs after the treatments showed no obvious biological toxicity (Figure S9), but H&E and TUNEL staining of tumor tissues revealed obvious nuclear damage in most tumor cells and cell death after treatment of the mice with $SNP_{DOX/CUR}$ (Figure 6(g)).

4 Conclusions

In summary, a simple dual-drug delivery system with a controllable and flexible drug release ratio was successfully constructed to deliver two anticancer drugs, DOX and CUR, for synergistic cancer therapy. The polymers PEG-ss-DOX and PEG-ss-CUR can self-assemble into nanoparticles and release loaded drugs at predefined ratios after responding to the high GSH levels in cancer cells due to synchronous drug activation and nanocarrier collapse. Drug release at predefined ratios endowed $SNP_{DOX/CUR}$ with the strongest synergistic effect at all drug effect levels and a much more significant tumor inhibition rate than traditional $ENP_{DOX/CUR}$. As a result, the dual-drug delivery system with a controllable and flexible drug release ratio developed in our work provides a simple and efficient strategy for combination chemotherapy with precise drug ratios.

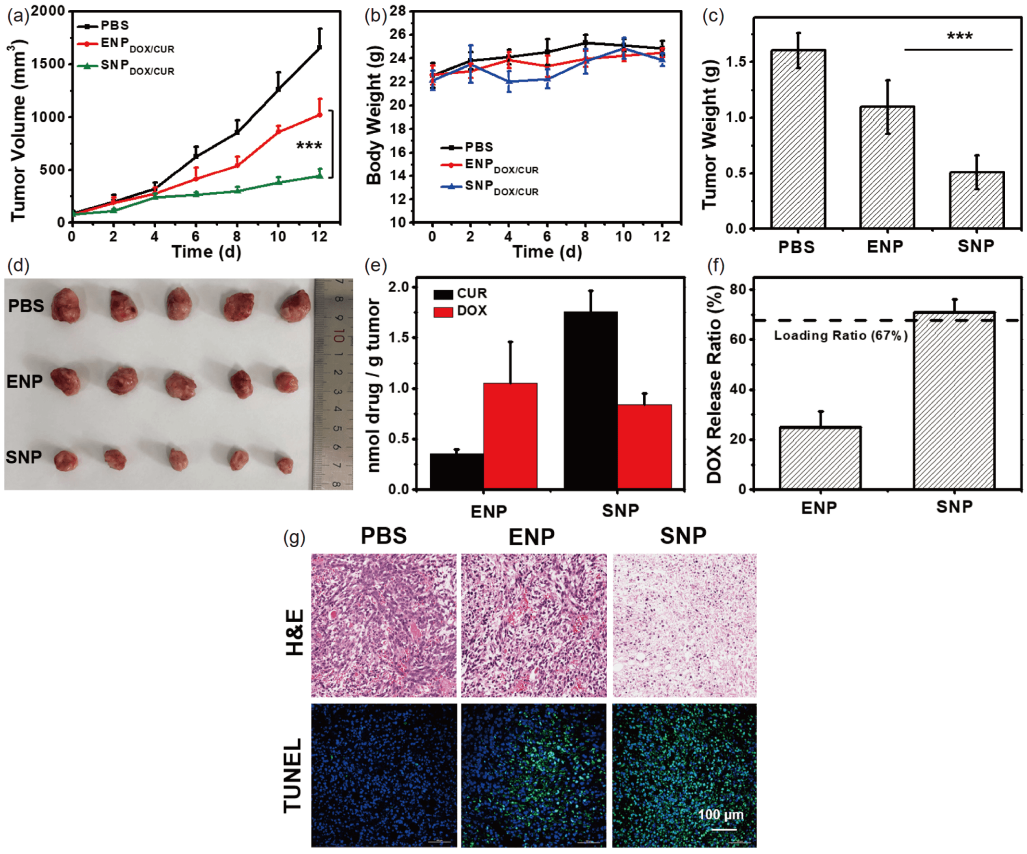

Figure 6 (a) Antitumor efficacy of intravenous administration of PBS, $ENP_{DOX/CUR}$ and $SNP_{DOX/CUR}$ in MCF-7/ADR tumor-bearing nude mice (n=5); (b) body weight changes in MCF-7/ADR tumor-bearing mice over time after different treatments; (c) quantitative analysis of tumor weights after different treatments; (d) photos of excised tumors; (e) quantitative analysis of free DOX and CUR concentrations in tumors; (f) the ratio of drugs released in tumors after different treatments (n=3); (g) H&E and TUNEL staining of tumor sections (color online).

Acknowledgements This work was supported by the National Natural Science Foundation of China (51873072, 52073101), Guangdong Provincial Pearl River Talents Program (2019QN01Y088), the Science and Technology Program of Guangzhou (202002030268, 201804020060), and Outstanding Scholar Program of Bioland Laboratory (Guangzhou Regenerative Medicine and Health Guangdong Laboratory) (2018GZR110102001).

Conflict of interest The authors declare no conflict of interest.

Supporting information The supporting information is available online at http://chem.scichina.com and http://link.springer.com/journal/11426. The supporting materials are published as submitted, without typesetting or editing. The responsibility for scientific accuracy and content remains entirely with the authors.

1 Monsuez JJ, Charniot JC, Vignat N, Artigou JY. *Int J Cardiology*, 2010, 144: 3–15
2 Xiao Q, Zhu W, Feng W, Lee SS, Leung AW, Shen J, Gao L, Xu C. *Front Pharmacol*, 2018, 9: 1534
3 Rawal S, Patel MM. *J Control Release*, 2019, 301: 76–109
4 Heinhuis KM, Ros W, Kok M, Steeghs N, Beijnen JH, Schellens JHM. *Ann Oncology*, 2019, 30: 219–235
5 Qin SY, Cheng YJ, Lei Q, Zhang AQ, Zhang XZ. *Biomaterials*, 2018, 171: 178–197
6 Jia J, Zhu F, Ma X, Cao Z, Cao ZW, Li Y, Li YX, Chen YZ. *Nat Rev Drug Discov*, 2009, 8: 111–128
7 Greco F, Vicent MJ. *Adv Drug Deliver Rev*, 2009, 61: 1203–1213
8 Lee SM, O'Halloran TV, Nguyen SBT. *J Am Chem Soc*, 2010, 132: 17130–17138
9 Houdaihed L, Evans JC, Allen C. *Mol Pharm*, 2018, 15: 3672–3681
10 Hu CMJ, Aryal S, Zhang L. *Therapeutic Deliver*, 2010, 1: 323–334
11 Spring BQ, Bryan Sears R, Zheng LZ, Mai Z, Watanabe R, Sherwood ME, Schoenfeld DA, Pogue BW, Pereira SP, Villa E, Hasan T. *Nat Nanotech*, 2016, 11: 378–387
12 Wang H, Zhao Y, Wu Y, Hu Y, Nan K, Nie G, Chen H. *Biomaterials*, 2011, 32: 8281–8290
13 Cui Y, Xu Q, Chow PKH, Wang D, Wang CH. *Biomaterials*, 2013, 34: 8511–8520
14 Vicent MJ, Greco F, Nicholson RI, Paul A, Griffiths PC, Duncan R. *Angew Chem Int Ed*, 2005, 44: 4061–4066
15 Chen H, Pazicni S, Krett NL, Ahn RW, Penner-Hahn JE, Rosen ST, O'Halloran TV. *Angew Chem Int Ed*, 2009, 48: 9295–9299
16 Liao L, Liu J, Dreaden EC, Morton SW, Shopsowitz KE, Hammond PT, Johnson JA. *J Am Chem Soc*, 2014, 136: 5896–5899
17 Pathak RK, Dhar S. *J Am Chem Soc*, 2015, 137: 8324–8327
18 Zhou F, Wang P, Peng Y, Zhang P, Huang Q, Sun W, He N, Fu T, Zhao Z, Fang X, Tan W. *Angew Chem Int Ed*, 2019, 58: 11661–11665
19 Lin S, Xie P, Luo M, Li Q, Li L, Zhang J, Zheng Q, Chen H, Nan K. *Nano Res*, 2018, 11: 3619–3635
20 Camacho KM, Kumar S, Menegatti S, Vogus DR, Anselmo AC, Mitragotri S. *J Control Release*, 2015, 210: 198–207
21 Sagnou M, Novikov FN, Ivanova ES, Alexiou P, Stroylov VS, Titov IY, Tatarskiy VV, Vagida MS, Pelecanou M, Shtil AA, Chilov GG. *Eur J Med Chem*, 2020, 198: 112331
22 Iyer AK, Khaled G, Fang J, Maeda H. *Drug Discovery Today*, 2006, 11: 812–818